

Evolution of Phases, Microstructure, and Surface Roughness during Heat Treatment of Aluminized Low Carbon Steel

FRANK JENNER, MARK E. WALTER, RAJ MOHAN IYENGAR, and RON HUGHES

Diffusion processes for aluminum-silicon coatings on low carbon sheet steels during austenizing have been investigated. Temperature profiles were imposed with closed-loop control of a motorized linear slide that moves samples through a tube furnace. Heat treatment variables were heating rate, hold temperature, and hold time. Subsequent analysis included scanning electron microscopy (SEM), energy dispersive X-ray spectroscopy (EDS), and surface roughness measurements. The evolution of the coating was tracked by following the formation of seven main microstructural regions. In order to observe the cross-sectional microstructure without any mechanical influence of the preparation process, a focused-ion beam (FIB) was used. The effects of the various heat treatment parameters were evaluated. The resulting observations and data enhance the understanding of the diffusion process and provide information needed to optimize the heat treatment.

DOI: 10.1007/s11661-009-0105-x

© The Minerals, Metals & Materials Society and ASM International 2010

I. INTRODUCTION

ONE of the important ways to improve fuel economy is to reduce the mass of automotive vehicles. The mass reduction should, however, not compromise the vehicle crashworthiness that influences passenger safety. Hence, ultra-high-strength sheet metals such as heat-treatable boron steels are increasingly used.^[9] This class of steels has low carbon content, is microalloyed, and is quenchable, thereby leading to ultra high strength after the component is stamped.^[14,16] Steel sheets are austenized at about 1173 K (900 °C) to 1223 K (950 °C) in a continuous feed furnace and then transferred to a die where the forming and subsequent quenching takes place. Complex shapes and high strength can be achieved with one stroke.^[3] In order to improve the corrosion resistance and paintability after the component is formed, as well as to prevent scaling and decarburization during the heat treatment, an aluminum-silicon (Al-Si) coating with 7 to 11 pct Si is applied before hot forming.^[9,11,16] A common process for aluminizing is hot dipping.^[15] This article will focus on the behavior of the hot-dipped coating during the heat treatment, prior to the forming operation.

II. LITERATURE REVIEW

Al-Si coatings with 7 to 11 pct silicon are known as “type 1” coatings, whereas aluminum coatings without silicon are referred to as “type 2” coatings. In addition to their application in high-strength sheet steels for hot forming, aluminized type 1 coatings are used for elevated temperature applications and applications requiring significant corrosion resistance. Several researchers have focused mainly on the latter applications and have investigated long-term diffusion, corrosion resistance, hot dip parameters such as immersion time, and as-coated alloy layer growth.^[15]

Richards *et al.*^[15] states that as long as the aluminum concentration remains above a critical value, corrosion resistance is provided through a protective oxide layer,^[15] whereas the addition of silicon reduces the corrosion resistance slightly and the coating may undergo pitting corrosion.^[4] The coating weight of type 1 coatings is typically 15 to 25 μm per side (about 75 to 120 g/m^2).^[15] During hot dipping, a thin alloy layer forms between the substrate and the Al-Si coating. For postdip forming operations, a thinner alloy layer is less susceptible to cracking and, hence, more favorable.^[15] Inside the soft Al-Si matrix, isolated Fe-Al-Si intermetallic inclusions appear in the shape of platelets or dendrites.^[8,15] Depending on the deformation level, composition, and interfaces of the coating and the substrate, the alloy layer starts growing between 633 K (360 °C) and 853 K (580 °C). Quantifying alloy layer growth is difficult because of the spalling of the coating and the formation of jagged interfaces.^[5,15]

Although various intermetallics form in the alloy layer during heat treatment, Fe_2Al_5 is a main component.^[8] The intermetallics that form during diffusion are hard and brittle.^[15] Fe_2Al_5 is practically nondeformable at room temperature.^[4] Intermetallics richer in aluminum are closer to the surface of the coating.^[1] Since

FRANK JENNER, Graduate Student, and MARK E. WALTER, Professor, are with the Department of Mechanical Engineering, The Ohio State University, Columbus, OH 43210. RAJ MOHAN IYENGAR formerly Platform Manager with Advanced Engineering and Product Applications, Severstal North America, Dearborn, MI 48120, is currently with Component Integrity Branch, Office of Nuclear Regulatory Research, United States Nuclear Regulatory Commission, Mail Stop CSB-05A24M, Rockville, MD 20852. Contact e-mail: rmohan@severstalna.com RON HUGHES, Manager, is with Advanced Engineering and Product Applications, Severstal North America, Dearborn.

Manuscript submitted August 31, 2009.

Article published online April 1, 2010

intermetallics with higher aluminum contents have higher hardness and brittleness, iron-rich intermetallics are preferable.^[13] The brittleness and thermal expansion mismatch of the intermetallics results in coating cracks.^[6] High temperatures, oxide layers, or surface films that were not removed on the steel before hot dipping are believed to increase coating delamination.^[13,15]

The large number of possible phases in the binary Fe-Al and ternary Fe-Al-Si phase diagram, as well as possible metastable phases, makes the identification of coating phases quite challenging.^[15] It is hard to isolate phases^[10] and complex diffusion mechanisms associated with time constraints preclude equilibrium resulting in a wide variety of metastable phases.^[7] Energy dispersive X-ray spectroscopy (EDS) and X-ray diffraction (XRD) are often not accurate enough in determining the different phases.^[7,12] For more detailed information, sophisticated methods such as transmission electron microscopy,^[12] electron probe analysis,^[10] or microdiffraction with a focused XRD^[7] are necessary. Hence, the information on some phases is sparse and emphasis was placed only on the aluminum-rich corner of the Fe-Al-Si phase diagram.^[15] Therefore, phase identification in Al-Si coated steels has been a subject of controversy.^[1,4,15]

The kinetics of diffusion within the coating may not be significantly influenced by the steel substrate chemistry. Carbon and nitrogen can have an influence, since iron aluminides have a low solubility for those elements. A buildup of nitrogen or carbon-enriched zone slows the diffusion process. Therefore, the stabilization or control of interstitials is important to reduce the tendency toward coating delamination. Furthermore, this promotes the rapid transition to α -FeAl and precludes void formation. Titanium can be used to make the steel interstitial free with a side benefit of improvement in corrosion resistance. As a consequence, there is a faster alloy layer growth enabling improvement in formability. In addition to the steel composition, an austenitic structure aids the lower rate of alloying than a ferritic structure.^[15] Despite these influences on the coating, substrate composition is mostly dictated by noncoating related requirements. For example, boron heat-treatable steels need to contain a stoichiometric composition of titanium to tie up nitrogen, preventing the formation of boron nitrides and keeping the boron in solid solution to promote hardenability.

The alloy layer growth of aluminized coatings with silicon is significantly less than the growth for aluminized coatings without silicon. The optimum of alloy layer growth retardation is found to be around 9 wt pct silicon. For coatings without silicon, the *c*-axis of the Fe₂Al₅ orthorhombic unit cell consists completely of aluminum atoms, of which about 30 pct are vacant.^[15] The anisotropic unit cell results in directionally dependent diffusion processes. Silicon is assumed to occupy the vacancies on the *c*-axis and therefore greatly inhibits the alloy layer growth.^[15] Consequently, silicon reduces the activity coefficient of aluminum in type 1 coatings.^[1,5,10] Silicon also builds ternary phases that may slow the diffusion process. Silicon is known to increase dissolution and spalling of the coating layer.^[15]

III. EXPERIMENTAL

Hot-dipped steel sheets with a thickness of 1.7 mm are used for the experiments with different heat treatment parameters. The base metal chemistry is provided in Table I. The as-received sheets have a ferrite-pearlite structure. As shown in Figure 1, the initial coating thickness is about 30 μ m with an alloy layer thickness of less than 25 pct of the coating thickness. The sample size is 25 \times 25 mm.

A small scale heat treatment facility was designed to be able to simulate the temperature profiles used in production. As shown schematically in Figure 2, this custom heat treatment facility consists of a linear motion unit, a sample holder with a thermocouple that is in contact with the sample, two large metal blocks for quenching, and a tube furnace. The heating rate can be adjusted by varying the speed with which the sample is moved into the hotter section of the furnace. The thermocouple signal is used as feedback for closed loop proportional/integral/derivative (PID) control of the speed of the slide. Once the heat treatment is complete, the control system quickly moves the sample out of the furnace where it is quenched between two metal blocks.

The samples are then sectioned, ground, and polished with diamond compound. The preparation of aluminized steels for metallurgical analysis is a demanding task, which requires considerable experience. The challenge arises largely because of the brittleness of the intermetallic phases and of the differences in hardness

Table I. Typical Alloy Composition of the Boron Steel Used in This Study

C	Mn	P	Si	Cr	Al	S
0.2	1.23	0.011	0.258	0.217	0.043	0.005
Nb	Ti	V	Mo	B	N	Ca
0.003	0.038	0.017	0.003	0.003	0.015	0.003

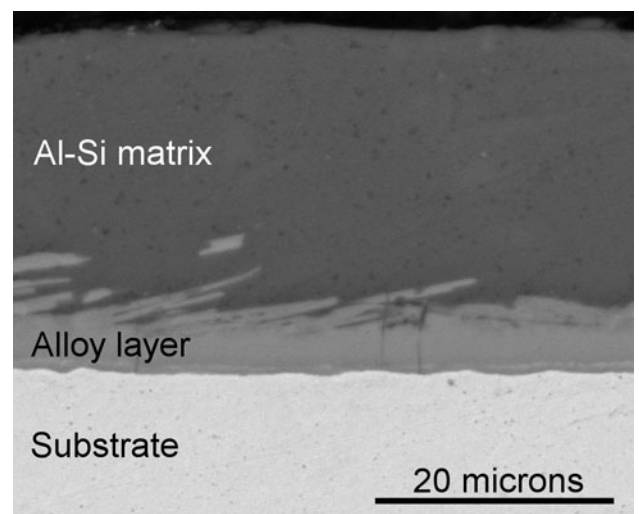


Fig. 1—SEM micrograph of the microstructure of the Al-Si coating before the heat treatment.

between the intermetallics and metal phases. Because of galvanic effects, preparation in aqueous media can lead to etch pits. Etching and chemical polishing react differently on the various phases and may bias the results. Consequently, the preferred preparation method is mechanical polishing.^[13] A recommendation for specimen preparation is provided in the *ASM Handbook*.^[17]

The microstructure is analyzed with scanning electron microscopy (SEM). Some sample cross-sectional images are further processed by a custom image processing program. The images are segmented according to the gray level, and the segmented regions are analyzed to determine the volume fractions. The EDS line scans are similarly divided into regions. The combination of SEM images and of EDS line scans enables the determination of compositional ranges for each region.

The surface roughness is analyzed with a Veeco Wyko optical profiler (NT3300, Veeco Instruments Inc., Plainview, NY). The noncontact profiler makes three-dimensional (3-D) measurements of the topography. The surface profile is determined using optical phase shifting and white light vertical scanning interferometry. Digital postprocessing generates an image of the surface profile providing valuable information on surface roughness.

The roughness measurements presented are based on a scanning size of $225 \times 296 \mu\text{m}$. The data are not filtered. For measurement spots with steep inclinations, the optical profiler cannot measure the surface height properly. Those spots are black in the surface profile image. Depending on the aim of the surface characterization, the measurement scale is important. The optical profiler is commercially used to characterize the surface profile with respect to paint adherence and tribology.

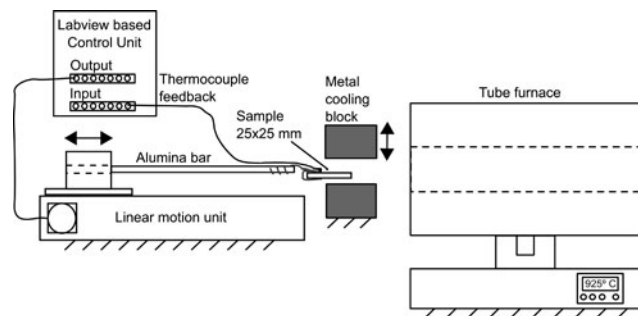


Fig. 2—Schematic view of the custom heat treatment facility.

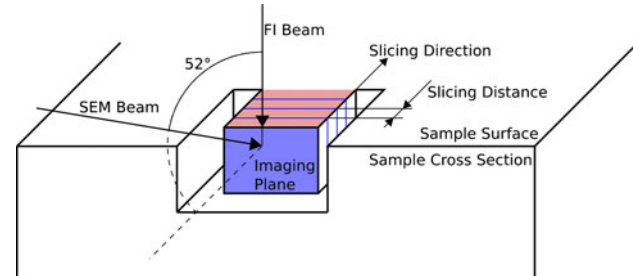


Fig. 3—Serial sectioning with dual-beam FIB-SEM.

Voids are investigated using SEM cross-sectional images. The polishing damage of the cross section is verified with a focused ion beam (FIB)–SEM dual beam FEI Nova 600. Before the FIB is applied, a thin film of platinum is deposited on the surface of the coating. This improves the smoothness of the imaging plane. The FIB can remove very fine slices of material and is used for serial sectioning of the coating (Figure 3). After each slice is removed, an SEM backscatter image is taken. The angle between the two beam columns is 52 deg, and the slicing distance is set to $0.5 \mu\text{m}$. The generated image series shows the 3-D microstructure without mechanical alteration. Through postprocessing, the images are resized to adjust the distortion arising due to the nonperpendicular angle between the SEM beam and the imaging plane.

IV. COATING EVOLUTION OF MAIN MICROSTRUCTURAL REGIONS

In order to explore the diffusion process over time, heat-treated samples with temperature profiles as shown in Figure 4 were produced. The heating rate of 283 K/s ($10 \text{ }^\circ\text{C/s}$) and furnace temperature of 1198 K ($925 \text{ }^\circ\text{C}$) were constant for all the samples in Figure 4. The time shown next to each temperature profile is the time measured from the start of heating until the sample is moved out of the furnace. The samples with less than 105 seconds have highly reflective metallic surfaces, while all the other samples have dull, matt surfaces. Differences in color, ranging from dark blue to pinkish brown, are observed on the surface depending on the hold times. Very long hold times appear to give rise to pinkish brown regions on the surface.

Phases with different densities can be distinguished by SEM backscatter imaging. Backscatter SEM images of the cross sections show various different phases that are differentiated by the intensity of gray levels. Because there are many phases that may differ only slightly, the microstructure is divided into regions. It is assumed that even if one region consists of several phases, the basic properties of these phases are comparable and the

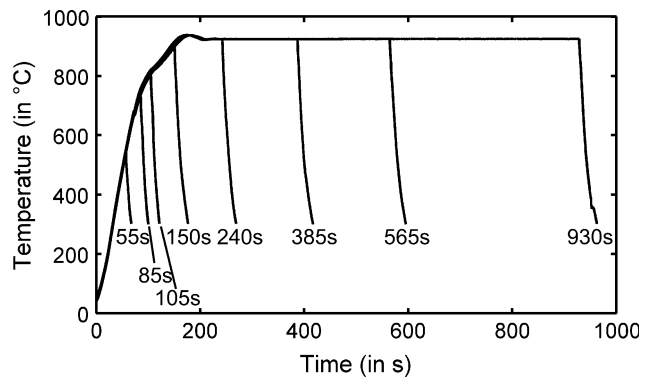


Fig. 4—Temperature profiles for the variation of the heat treatment time. The furnace temperature was 1198 K ($925 \text{ }^\circ\text{C}$), and the heating rate was 283 K/s ($10 \text{ }^\circ\text{C/s}$).

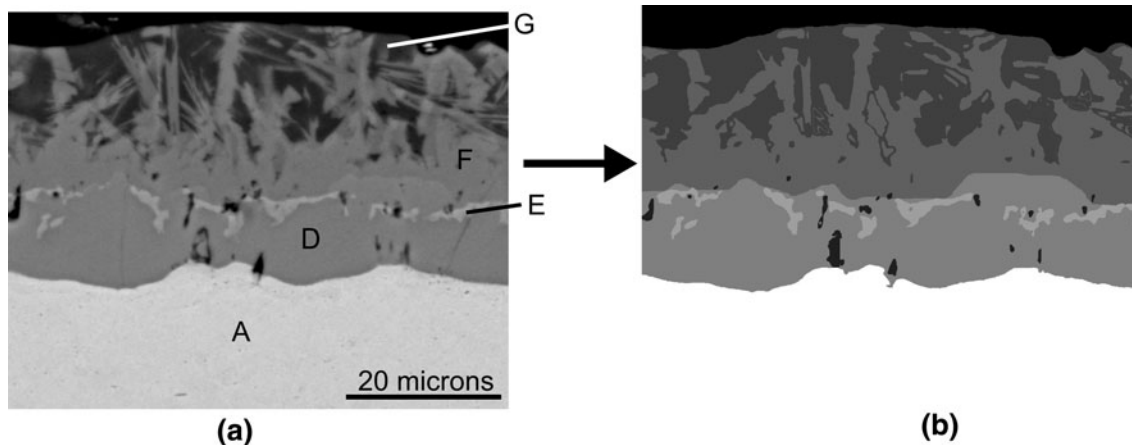


Fig. 5—Microstructure after interrupting heat treatment at 150 s: (a) actual micrograph and (b) processed image.

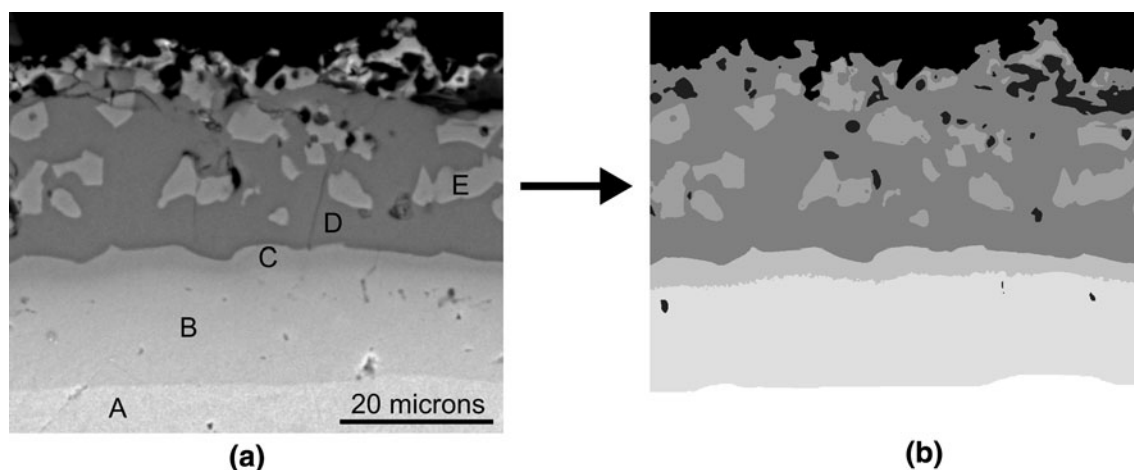


Fig. 6—Microstructure after interrupting heat treatment at 565 s: (a) actual micrograph and (b) processed image.

regions are treated as one unit. The SEM micrographs and processed images for heat treatments (interrupted at 150 and 565 seconds) are shown in Figures 5 and 6, respectively.

As shown in Figures 5 and 6, each region is designated with letters A through G. The letters are ordered from the substrate to the surface. The letter A is the substrate and G is the Al-Si matrix. The different alloy layers are denoted B through F. It should be mentioned that not all layers always appear, because either they might have not yet formed or they are too small to be visible. Generally, it is observed that the interfaces (boundary) of the denser regions such as A, B, and C are smoother, whereas the interfaces between D, F, and G are very irregular.

A selection of SEM images of samples with varying heat treatment time is shown in Figure 7. Analyzing the volume fractions of multiple SEM images leads to Figure 8. Based on the plots in Figure 8, the development of the coating is described as follows. For the given heating rate and hold temperature, regions B and C start emerging after about 150 seconds. Regions B and C are iron rich and their volume fraction increases steadily

over time. Regions D and E are aluminum and iron rich. These regions grow between 90 to about 250 seconds to a maximum volume fraction of about 70 pct. After 250 seconds, the volume fractions of regions D and E decrease. When considering region E by itself, it is observed that the volume fraction of E steadily increases. Region E is composed of silicon-rich precipitates within region D. It is believed that, because of the higher density of region E, once precipitated, its relative motion is restricted as the coating evolves further. Region F is aluminum rich. Because of the different gray levels within region F, it is assumed that F consists of several different intermetallics. Region F is already visible in as-coated samples and grows further after a critical temperature of about 823 K (550 °C) is exceeded. The volume fraction of region F peaks at about 150 seconds; it is then consumed by other phases and eventually disappears. Region G is the remainder of the solidified original Al-Si hot dip coating. Within 240 seconds, the Al-Si matrix is completely consumed by the alloy layer.

The stoichiometric density values for some of the common intermetallics are given in Table II. With these known densities, the volume fractions in Figure 8, and

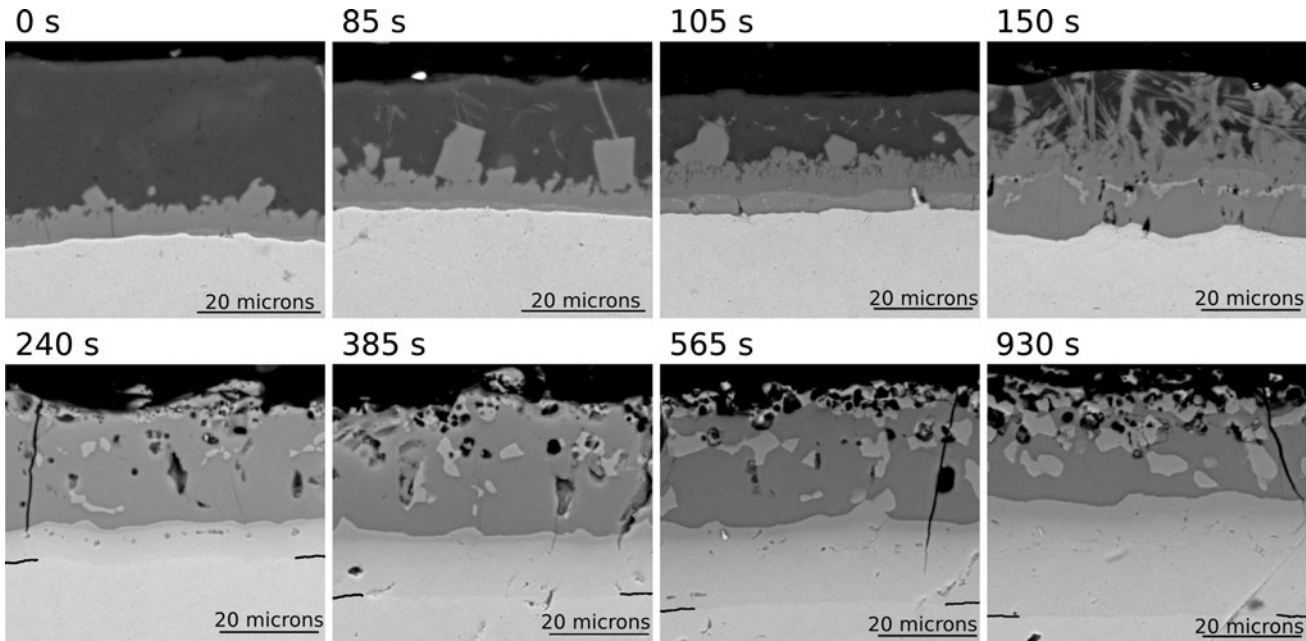


Fig. 7—Development of the coating microstructure over time. The temperature path of samples is shown in Fig. 4.

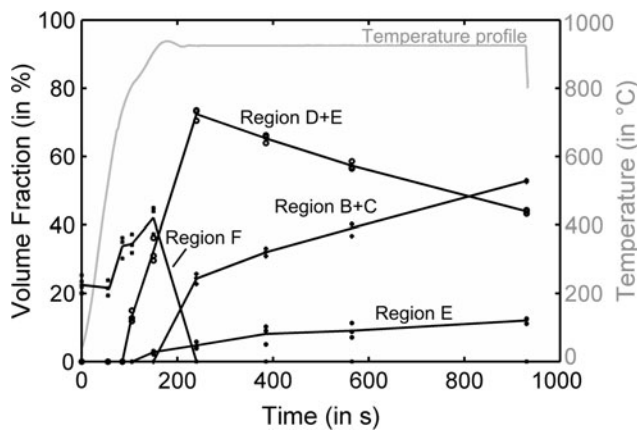


Fig. 8—Time evolution of the volume fractions of various regions. The temperature profile is given as a reference.

Table II. Density Values of Common Intermetallics^[6,15]

Intermetallic	Fe ₂ Al ₅	FeAl ₃	Fe ₂ SiAl ₈	FeAl
Density (g/cm ³)	4.11	3.9	3.62	5.37

the initial coating thickness and composition, a basic mass balance can be calculated. The initial thickness of the coating is assumed to be 30 μm . In the calculations, an average thickness for each region based on SEM images is used. The contribution of voids to the average density of the regions is neglected. Nonequilibrium and nonstoichiometric structural and compositional effects are also neglected in this calculation.

The mass balance helps to track where the material is moving during the heat treatment. The resulting through-thickness temporal evolution of the coating

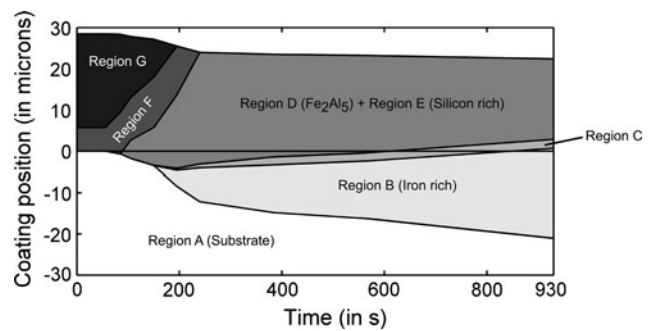


Fig. 9—Schematic time evolution of the coating as determined from the calculated mass balances. The y-axis gives an absolute reference for the position and thickness of regions.

regions is shown in Figure 9. In accordance to the mass balance, the aluminum content of the coating in Figure 9 always adds up to the initial coating weight. Figure 9 shows that the coating as a whole is moving inward, which is in accordance to the fact that the average density of the coating is increasing. It is believed that, even though heat treatment parameter variations may shift the phase ratios, any conventionally heat-treated sample can be located somewhere in Figure 9.

Several assumptions have been used in arriving at the evolution of the coating layers shown in Figure 9. The average densities for each region are calculated based on one-dimensional (through-thickness) measurements of the extent of various regions and the densities of predominant phases in these regions. Certainly, this assumption ignores the in-plane, as well as out-of-plane, variations of the sizes of the regions. Additionally, any contribution, *albeit* small, from other alloying elements in the substrate is not considered. Thus, the evolution of coating regions shown in Figure 9 is not strictly

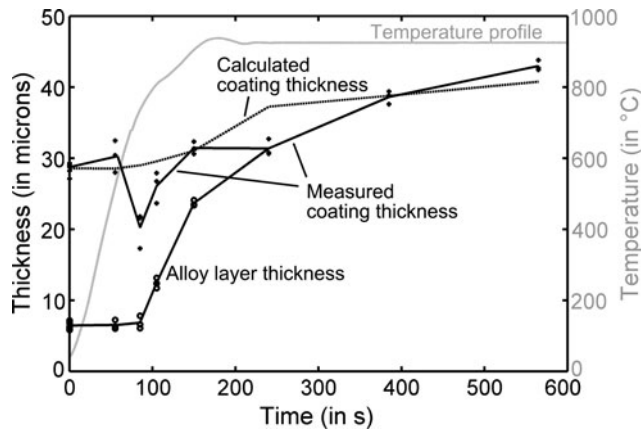


Fig. 10—Time evolution of the coating thickness and alloy layer thickness.

rigorous. Nonetheless, it does offer a qualitative picture of the complex evolution of the coating layer.

As illustrated in Figure 10, the coating thickness increases over time. The coating thickness is measured from where the SEM backscatter images indicate a changed substrate microstructure to the midregion of any surface undulation. The increase in coating thickness is a direct result of the formation of complex intermetallics due to the diffusion-aided process. The calculated coating thickness is also included in Figure 10. The calculated thickness is based on the volume fraction and region density data combined with the assumed initial coating thickness of 30 μm . The drop in measured coating thickness between about 60 and 100 seconds is believed to be an artifact caused by localized variations in the initial coating weight. Due to the assumption of uniform initial coating thickness, the calculation shows that the coating thickness is steadily increasing over time. Figure 10 also shows that within 240 seconds the alloy layer has completely consumed the Al-Si matrix.

The chemical composition of regions is measured with EDS. Because one region may consist of several phases, it is not possible to give the exact composition. Instead, for each region, Figure 11 presents the compositional ranges of the three main elements. It is noted that the silicon distribution in region G varies over a wide range. This wide range is the result of most of the silicon being concentrated in smaller precipitates. Thus, some EDS scan spots detected almost no silicon and other spots detected more than 50 pct silicon. A comparison of the EDS results and commonly reported binary Fe-Al and ternary Fe-Al-Si phases^[10,15] yields what phases are likely to be present. Some of the more important phases that are reported and that overlap with the measured compositional ranges are also shown in Figure 11 (a traditional equilibrium diagram).

The binary phases are plotted as lines that represent the solubility range of silicon at 1173 K (900 °C).^[10] The soluble silicon is assumed to replace aluminum; hence, the iron content is constant for binary phases. It should be kept in mind that Figure 11 is based on a

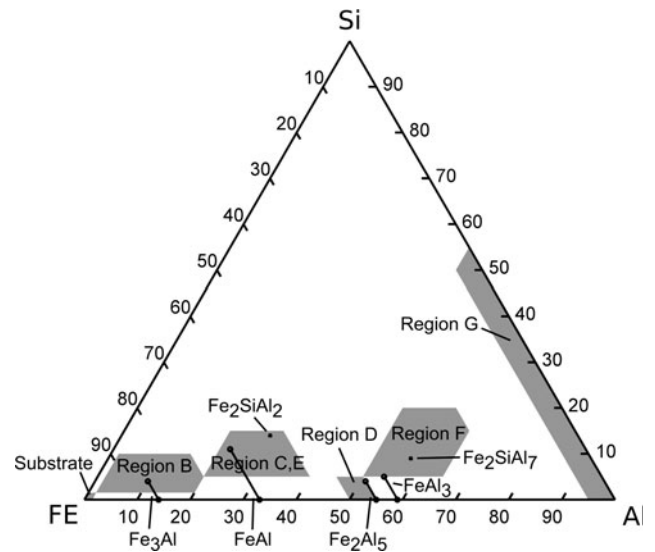


Fig. 11—EDS results showing the compositional ranges (weight percent) for each region. Also shown are commonly reported binary and ternary phases. The letters are ordered as the regions appear from the substrate (A) to the Al-Si matrix (G).

compositional analysis and neglects the complex nonequilibrium thermodynamics that influence the formation of compounds.

Using the results of other researchers^[1,10,15] and the current SEM microstructure and EDS results, the following regions are identified. Region A is defined as the substrate, where no significant diffusion of aluminum or silicon takes place. Region B is a solid solution of aluminum and silicon in iron. The compound Fe_3Al is also found inside this region. Regions C and E have the same compositional range, which includes FeAl and Fe_2SiAl_2 . As confirmed by electron backscatter diffraction, region D is identified as mainly Fe_2Al_5 . Fe_2Al_5 has a limited solubility for silicon. Hence, several silicon-rich phases precipitate inside region D. These silicon-rich phases are called region E. All other phases that develop between Fe_2Al_5 and the Al-Si matrix are called region F. These phases are aluminum rich. Finally, the solidified aluminum and silicon region that has a negligible amount of intermetallics with iron is denoted as region G.

The effects of heating rate and hold temperature on the evolved coating layer reinforce the validity of the evolution process described previously. The diffusion process is highly temperature dependent. Thus, as shown in Figure 12, it is not surprising that the microstructural evolution is accelerated by a higher hold temperature. The heat treatment times for the left, Figure 12(a), and right, Figure 12(b), samples were nearly the same. However, the thickness of region B for the right sample, Figure 12(b), is larger than its counterpart in Figure 12(a), resulting in the further advancement of region C toward the surface. Figure 12 also indicates that the higher hold temperature can change the precipitation behavior in region E. Figures 13(a) and (b) show that no significant alloying takes place below about 853 K (580 °C). Even though the heat treatment time for the sample, shown in

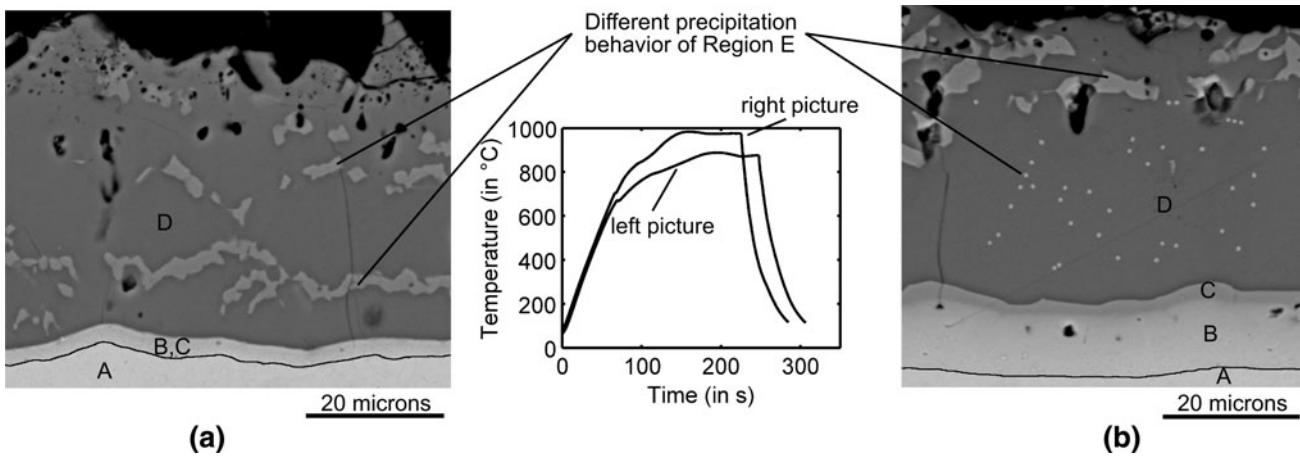


Fig. 12—Comparison of a hold temperature of (a) 1148 K (875 °C) and (b) 1223 K (950 °C). For better visibility, the interface A, B is redrawn. Also the bright spots within region D are accentuated.

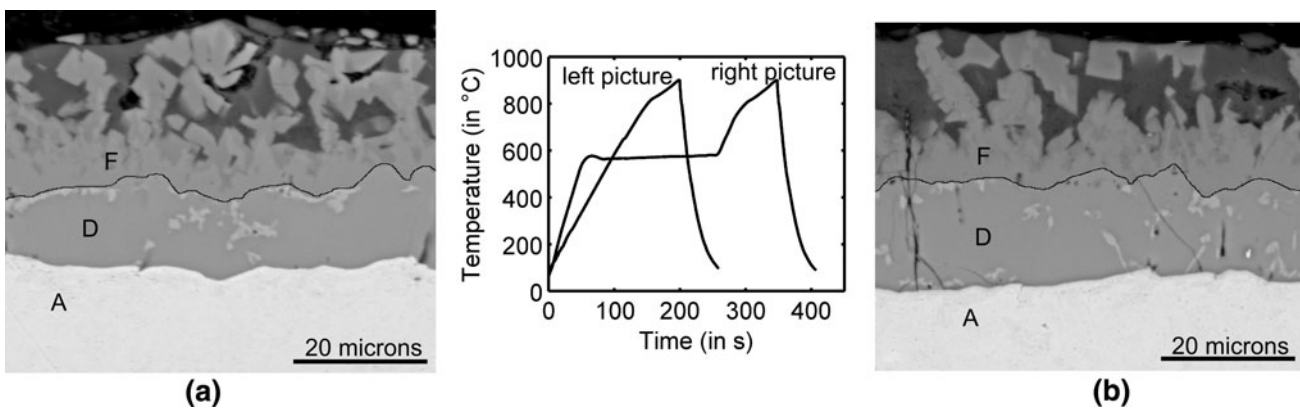


Fig. 13—Comparison of (a) a heating rate of 278 K/s (5 °C/s) and (b) a heating rate of 283 K/s (10 °C/s) that is at 843 K (570 °C) interrupted for about 200 s. For better visibility, the interface D, F is redrawn.

Figure 13(b), was much longer than that for the sample shown in Figure 13(a), only minor differences are evident.

The coating develops toward a microstructure with higher density, which for the given boundary conditions results in a change in volume of the coating. At the beginning, the coating mainly consists of a solidified Al-Si matrix and during the austenization this low density region transforms to high density iron aluminides (Figure 8 and Table II). Considering a constant number of atoms representing the entire coating and parts of the substrate, a change in average density will also change the volume those atoms occupy. For the given case, the average density of the coating is shown to increase, which translates to a volume reduction that was shown as the depression of the coating surface over time in Figure 9. The change in volume associated with the depression of coating surface (from the initial +30 μm) over time indicates a sharp decrease during the early stages followed by a very slow decrease (Figure 9). In subsequent plots showing the decrease in volume over time from Figure 9, the absolute value of the change is plotted. Recall that several assumptions

were used in the depiction of Figure 9. In particular, the contribution from voids to changes in the overall coating volume was not considered. Additionally, the inherent difficulty in accounting for the influence of surface roughness on the overall volume of the evolved coating precluded its consideration in the simplified calculation used to arrive at Figure 9. During the evolution of the coating layer, surface roughness changes and void initiation and growth are observed and will be discussed in more detail.

V. COATING LAYER EVOLUTION: SURFACE ROUGHNESS AND VOID FORMATION

In the case of surface roughness, it is assumed that the surface travels toward the substrate in order to reduce the volume in the formation of denser intermetallics. Ideally, materials will minimize their surface energy by developing a smooth surface. However, in real materials, the situation is complicated by energetic trade-offs between diffusion and surface tension, with precipitates playing a major role. As a result, for some spots, the

surface movement is hindered, while other spots can move more easily. A schematic of the surface roughening is shown in Figure 14.

The influence of the heat treatment on the surface profile is shown in Figure 15, where a sample shown in Figure 15(a) is as coated and a sample shown in Figure 15(b) is after the heat treatment. A certain degree of surface roughness is needed for better adhesion of paint systems used for automotive components.

For the samples of the heat treatment series presented in Figure 4, the surface roughness R_z is measured and plotted over time in Figure 16. Figure 16 also shows the change in volume that can be projected from the coating development model presented in Figure 9. For better comparison, the change in volume (absolute value) is plotted. Because the largest change in surface roughness coincides with the largest change in volume, a close dependence between surface roughness and volume change due to the formation of dense intermetallics is suggested.

In addition to understanding the principal dependence of coating development and surface roughness, it is of interest to determine how the temperature path in austenizing may influence the surface roughness. This helps to optimize the tribological properties during forming. An optimized surface roughness reduces tool wear and possibly improves paintability. Therefore, the influence of heating rates and hold temperatures on the evolution of surface roughness has been analyzed. Hold temperatures of 1223 K (950 °C) and 1173 K (900 °C) did not show a significant influence on surface roughness (Table III). However, varying the heating rate significantly affected the surface roughness. Comparing

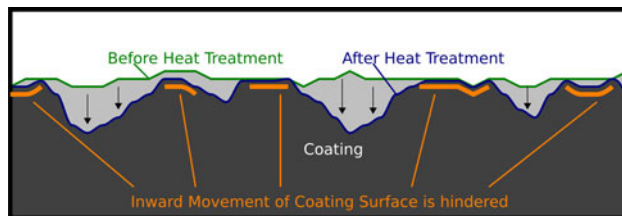


Fig. 14—Schematic figure of how surface roughness increases due to diffusion. Uniform light gray coating is prior to heat treatment. Dark gray roughened and partially heat treated coating is superimposed.

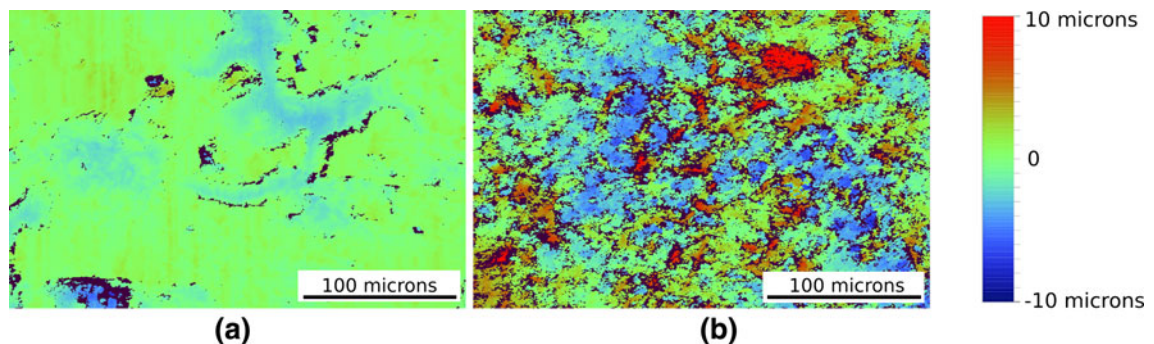


Fig. 15—Comparing the surface profile of (a) the sample as coated and (b) the sample heat treated (930 s with temperature path as shown in Fig. 4).

the samples with a heat treatment temperature path plotted in Figure 17, it can be seen that a higher heating rate resulted in a lower surface roughness (Figure 18 and Table III).

It has been suggested^[6,9] that void formation occurs during the heat treatment of type 1 Al-Si coatings and is thought to be the result of the Kirkendall effect due to the rapid diffusion of dominant species involved in the process. Hence, the term “Kirkendall voids” is attributed to the voids forming in the heat-treated coating layer. Because of the brittleness of the intermetallic coating, any mechanical polishing may induce damage to the coating resulting in voidlike features. It has not been unequivocally demonstrated whether the voids are

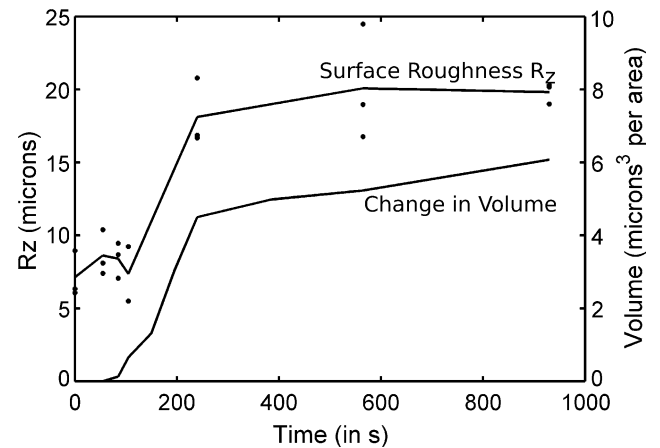


Fig. 16—Surface roughness (R_z) and change in volume over time.

Table III. Roughness Values R_z for Heating Profiles Shown in Figure 17

	Scan 1 (μm)	Scan 2 (μm)	Scan 3 (μm)
High heating rate	14.34	18.89	18.00
Hold temp.: 1223 K (950 °C)			
High heating rate (a)	18.35	18.10	17.48
Hold temp.: 1173 K (900 °C)			
Low heating rate (b)	29.95	29.43	26.39
Hold temp.: 1173 K (900 °C)			

inherent to the heat-treatment process or appear mainly due to damage caused by mechanical polishing. In this study, we use serial sectioning of the coating with a focused-ion beam (FIB) to conclusively show that voids appear in various shapes, sizes, and locations as a result of heat-treatment. With the FIB, it was possible to get SEM cross sectional images without any mechanical influence from polishing. Figure 19 shows an image series that follows a void region through the depth of the

material. Even though some voids have similar aspect ratios or are aligned in a row, most of the voids are just randomly distributed. The difficulties in recognizing patterns represent the complexity of diffusion and void forming mechanism.

Evaluating voids quantitatively is very challenging. First, an analytical description of void formation for most systems is not available. Second, the coating is fairly brittle and the preparation of microstructural cross sections poses a considerable challenge. Third, voids are randomly distributed with various shapes and sizes, most of them being small. Also, voids appear in SEM images in the same shading as the mounting material and cracks. This makes it difficult to have any image algorithm automatically recognize them. All of these factors contribute to a high variability within any results investigating voids.

Even though there is variability, it was possible to evaluate the void content semiquantitatively over time. Figure 20 compares the change in volume with the estimated void content over time. Since the highest increase in void content coincides with the highest change in volume, a correlation between those two variables is inferred. The void content and change in volume are both in the unit volume per surface area; hence, the two plots in Figure 8 are quantitatively comparable. The void content is far lower than the change in coating volume calculated based on the assumptions detailed earlier in the article. This leads to

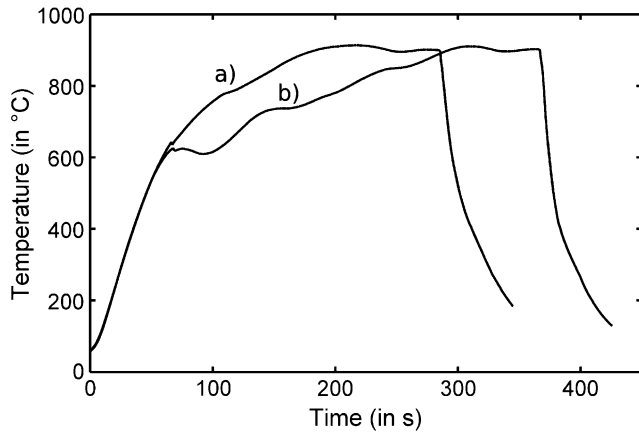


Fig. 17—Temperature path of two samples: (a) high heating slope and (b) low heating slope.

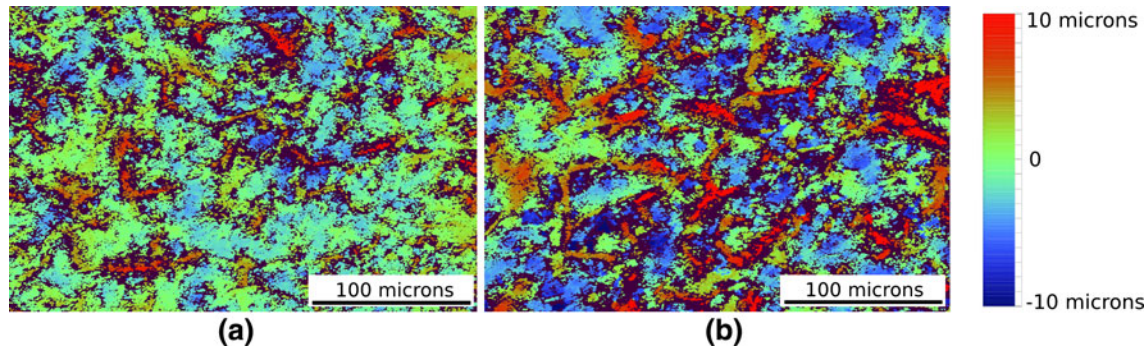


Fig. 18—Comparing the (a) high heating rate and (b) lower heating rate at 1173 K (900 °C), it is seen that the surface roughness of condition (a) is significantly lower.

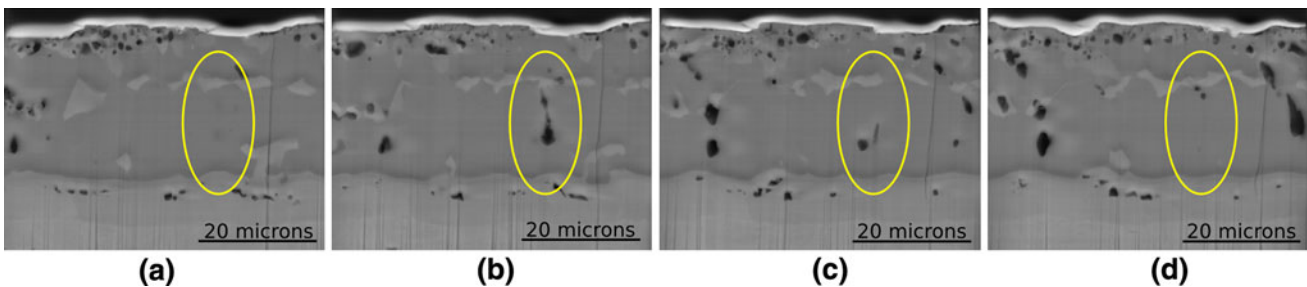


Fig. 19—Sequential FIB/SEM images of heat-treated Al-Fe-Si coating in boron steels. Image series that follows a void region through the depth of the material. Between each cross section, there is a difference in depth of 1.5 μm .

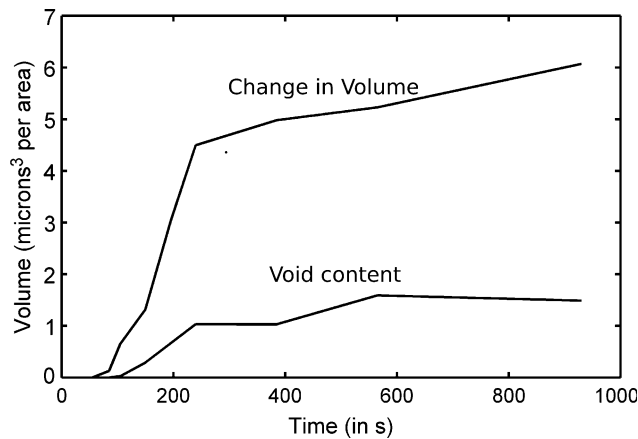


Fig. 20—Schematic comparison between change in volume and void content for heat-treated Al-Fe-Si coating in boron steel.

the inference that the void formation contributes a smaller part relative to the volume changes associated with the evolution of surface roughness.

The effects of different heat treatments on the reduction or promotion of voids have been investigated. In the scope of this investigation, it was not possible to determine a temperature profile that fulfills the requirements related to hot forming with simultaneous reduction of voids. Even though most studies observe voids and some relate them with Kirkendall voids,^[6,9] scant information is available for void properties and void formation of aluminum-silicon coatings. However, Richards *et al.*^[15] indicate that changing boundary conditions may change the void content. For example, a reduction of voids is observed when expedited alloying in the coating is enabled through addition of titanium. On the other hand, prestrain appears^[15] to enhance void formation.

VI. CONCLUSIONS

There are various challenges associated with understanding diffusion processes. The complex coating microstructure consists of numerous binary and ternary phases that are difficult to identify. Hence, the main microstructural regions are defined and compositional ranges are presented. In addition, the coating evolution during an austenizing heat treatment is described. The results show that the brittle and aluminum-rich intermetallics, typical of regions D and F, form mainly at the beginning of the heat treatment, while the phases richer in iron, represented in regions B, C, and E, emerge later on. The imposed temperature profile influences the speed at which the evolution of the coating takes place and the precipitation behavior of some regions, such as region E.

Furthermore, it is experimentally shown that the evolution of surface roughness as well as the increase in void volume accompany the reduced volume of the coating due to the formation of denser intermetallics. It is unequivocally demonstrated, through serial sectioning of the coating with a FIB, that void formation is inherent

during the evolution of the intermetallic coating. The content of the voids, however, is small in relation to the overall coating region. Measurements also show that the surface roughness can be influenced by the temperature path during austenizing. The results do not demonstrate a clear functional dependence between hold temperature, hold time, or heating rate and evolution of voids, because the quantification of voids has some uncertainties. The temperature path that would change the void content significantly could not be determined. However, published research work^[15] indicates that changing the boundary conditions influences the amount of voids.

The results show the relation between temperature path, microstructure, change of volume, surface roughness, and void content. It is the subject of ongoing research to evaluate the effects of these factors on the mechanical performance of the coating as well as weldability and paintability.

ACKNOWLEDGMENTS

The authors express their gratitude to Christopher Kristock (SNA) and Pat Pendleton and Dick Nester (Wheeling-Nisshin) for their encouragement and support. The authors acknowledge the funding and support of Severstal North America.

REFERENCES

1. M.V. Akdeniz, A.O. Mekhrabov, and T. Yilmaz: *Scripta Metall. Mater.*, 1994, vol. 31, pp. 1723–28.
2. P. Akerstrom and M. Oldenburg: *J. Mater. Process Technol.*, 2006, vol. 174, pp. 399–406.
3. T. Altan: *Stamping J.*, 2006, Dec., pp. 40–41.
4. A. Bahadur and O. Mohanty: *Metall. Trans.*, 1991, vol. 32, pp. 1053–61.
5. J. Barros, T. Ros-Yanez, and Y. Houbaert: *Defect Diffus. Forum*, 2005, vols. 237–240, pp. 1115–20.
6. Y.Y. Chang, C.C. Tsaur, and J.C. Rock: *Surf. Coat. Technol.*, 2006, vol. 200, pp. 6588–93.
7. P. Dillmann, B. Regad, and G. Moulin: *J. Mater. Sci. Lett.*, 2000, vol. 19, pp. 907–10.
8. N.A. El Mahallawy, M.A. Taha, M.A. Shady, A.R. ElSissi, A.N. Attia, and W. Reif: *Mater. Sci. Technol.*, 1997, vol. 13, pp. 832–39.
9. D.W. Fan, H.S. Kim, S. Biroasca, and B.C. De Cooman: *Proc. Materials Science and Technology 2007*, Detroit, MI, Sept. 16–20, 2007, Materials Science and Technology (MS&T), Westerville, OH, 2007, pp. 99–110.
10. S.P. Gupta and T. Maitra: *Mater. Charact.*, 2003, vol. 49, pp. 269–91.
11. P. Hein, R. Kefferstein, and Y. Dahan: *New Development in Sheet Metal Forming Technology*, Proc. Int. Conf., Stuttgart, Germany, Universität Stuttgart, Stuttgart, Germany, 2006, pp. 163–75. <http://www.uni-stuttgart.de/ifu/publikationen/tagungsbaende/index.en.html>.
12. K. Kee-Hyun, B. Van-Daele, G. Van-Tendeloo, and Y. Jong-Kyu: *Mater. Sci. Forum*, 2006, vols. 519–521, pp. 1871–75.
13. S. Kobayashi and T. Yakou: *Mater. Sci. Eng.*, 2002, vol. A338, pp. 44–53.
14. A. Merklein and J. Lechler: *J. Mater. Process. Technol.*, 2006, vol. 177, pp. 452–55.
15. R.W. Richards, R.D. Jones, P.D. Clements, and H. Clarke: *Int. Mater. Rev.*, 1994, vol. 39 (5), pp. 191–212.
16. M. Suehiro, K. Kusumi, T. Miyakoshi, J. Maki, and M. Ohgami: Nippon Steel Report No. 88, Nippon Steel, Tokyo, Japan, 2003.
17. ASM Materials Information [electronic resource], ASM Handbooks Online, 2007, www.asminternational.org.